# Application of the Finite-Difference Time-Domain Method to Radiation from Shielded Enclosures

D. M. Hockanson, J. L. Drewniak, T. H. Hubing, and T. P. VanDoren
Department of Electrical Engineering
University of Missouri–Rolla
Rolla, Missouri, 65401

## Abstract

The finite-difference time-domain method is applied to the analysis of radiation from shielding enclosures with internal sources. Results from the three-dimensional code which has been developed are compared with analytical results from waveguide problems and the Lawrence Livermore TSAR code. Two enclosure examples are given to demonstrate the utility of the FDTD method for this application. One example is for radiation from slots, and the other is coupling of energy from a nonresonant aperture to an attached shielded cable that results in enhanced radiation.

## 1 Introduction

The finite-difference time-domain (FDTD) method has found application in the analysis of many electromagnetic field problems including scattering, planar microwave circuits, and antennas [1], [2]. In each case, the FDTD method has proven to be an accurate full-wave analysis of the particular electromagnetic field problem investigated. The advances in computational power and speed within the past few years and the availability of high-speed desktop workstations, has made it possible to analyze many electromagnetic fields problems which previously might have been considered intractable. Among these are EMC and EMI problems. The FDTD method has many advantages for EMC problems including modeling of arbitrary inhomogeneities and lumped circuit elements. The FDTD method has been applied to EMC problems for investigating coupling through an aperture in a shielded enclosure to a wire [3], radiation from VLSI heatsinks [4], and two-dimensional radiation through air vents [5]. Because of the complexity of typical EMC problems, analytical solutions are often difficult at best. As a result, designs are often guided by maxims that are based on simple problems for which analytical solutions are available, or past experience. Numerical electromagnetic modeling of EMC problems offers the possibility of providing insight into design problems where intuition and experience may provide insufficient guidance.

A three-dimensional FDTD code has been developed to study radiation from shielding enclosures as well as printed circuit boards. The code, denoted APOGEE (Analytical Program for Observing General Electromagnetic Emissions) has the capabilities for modeling conductors, lossy dielectrics, wires, and several types of sources. Arbitrary geometries can be handled, however, since a rectangular mesh is employed, geometries that do not conform to a rectangular mesh must be approximated in a staircasing fashion. Results from the present work are compared to the Lawrence Livermore TSAR (FDTD) code as well as to analytical solutions for an inhomogeneously filled waveguide. APOGEE is employed to investigate radiation through multiple slots. Also studied is excitation of a shielded cable through an aperture of non-resonant dimensions in a shielded enclosure. It is shown that the radiation as a result of the attached cable is a function of the location of the cable around the aperture.

## 2 FDTD Modeling

The finite-difference time-domain method has been described in detail in the literature [2], [6], and is only briefly outlined here. Maxwell's curl equations in lossy regions with sources can be written as

$$\begin{aligned} \nabla \times \overline{\mathbf{E}} &= -\mu \frac{\partial \overline{\mathbf{H}}}{\partial t} - \rho_m \overline{\mathbf{H}} - \overline{\mathbf{M_i}} \\ \nabla \times \overline{\mathbf{H}} &= \epsilon \frac{\partial \overline{\mathbf{E}}}{\partial t} + \sigma_e \overline{\mathbf{E}} + \overline{\mathbf{J_i}} \end{aligned} \tag{1}$$

where $\overline{\mathbf{E}}$, $\overline{\mathbf{H}}$, $\overline{\mathbf{M_i}}$, $\overline{\mathbf{J_i}}$ are the electric field, magnetic field, impressed magnetic current density , and impressed electric current density vectors, respectively. The permeability and permittivity are represented by $\mu$ and $\epsilon$, and $\rho_m$ and $\sigma_e$ are the magnetic resistance and electric conductance of the medium. In rectangular coordinates, the vector equations can be written as six scalar equations. The z-component of the Ampere's law equation is given by

$$\epsilon \frac{\partial E_z}{\partial t} = \left( \frac{\partial H_y}{\partial x} - \frac{\partial H_x}{\partial y} \right) - \sigma_e E_z - J_{zi} \tag{2}$$

Each equation for the six vector components can be discretized using central differencing. Applying central differencing, which is accurate to second order, an explicit update equation for $E_z$ can be determined as

$$\begin{aligned} & E_z^{n+1}(i,j,k+\frac{1}{2}) \\ &= \frac{2\epsilon - \Delta t \sigma_e}{2\epsilon + \Delta t \sigma_e} E_z^n(i,j,k+\frac{1}{2}) + \frac{2\Delta t}{2\epsilon + \Delta t \sigma_e} \end{aligned} \tag{3}$$

0-7803-1398-4/94/0000-0014 $4.00 © 1994 IEEE

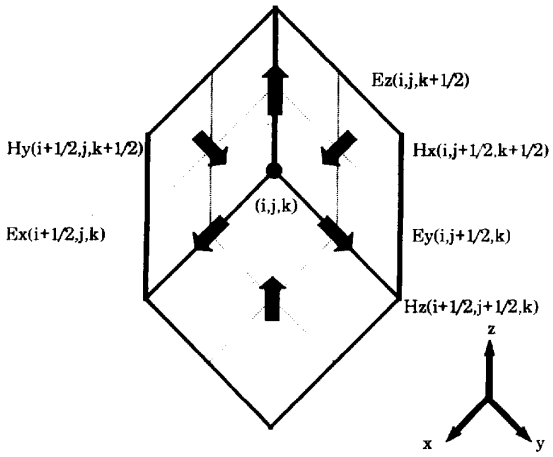


Figure 1: Unit cell for Yee's mesh.

$$\times \left\{ \frac{H_y^{n+\frac{1}{2}}(i+\frac{1}{2},j,k+\frac{1}{2}) - H_y^{n+\frac{1}{2}}(i-\frac{1}{2},j,k+\frac{1}{2})}{\delta x} \right.$$

$$- \frac{H_x^{n+\frac{1}{2}}(i,j+\frac{1}{2},k+\frac{1}{2}) - H_x^{n+\frac{1}{2}}(i,j-\frac{1}{2},k+\frac{1}{2})}{\delta y}$$

$$\left. - J_z^{n+\frac{1}{2}}(i,j,k+\frac{1}{2}) \right\}$$

Discretisation of the scalar equations requires the domain to be modeled as a mesh of rectangular cells with dimensions $\Delta x \times \Delta y \times \Delta z$. The corners of the cells are referenced as nodes located at coordinates $(i, j, k)$, and the time index is denoted by $n$. Similar equations can be developed for the remaining five vector components of the electric and magnetic fields.

The electric and magnetic field components are interleaved in space and distributed over a unit cell as shown in Fig. 1. The electric field components are located on the edges, and the magnetic field components are normal to the center of the faces. These cells are then stacked to fill the computational domain. Arbitrary geometries must be modeled in a staircased fashion due to the rectangular shape of the cells. In the work detailed herein, the domain is truncated with Mur's second order absorbing boundary conditions [8]. Edges of the computational domain are truncated with Mur's first order boundary condition, because second order equations require electric field components which are outside the domain at the edges. The electric and magnetic fields are not computed at the same time step, but rather are computed alternately. This 'leap-frogging' scheme is the basis for the Finite-Difference Time-Domain (FDTD) method.

Perfect electric conductors are modeled by setting appropriate tangential electric field components to zero at the location of a conductor surface. Within the computational domain, all conductors must be located on the electric field grid. Infinitesimally thin wires are similarly modeled by setting the tangential electric field component to zero along the wire axis for cells through which the wire passes.

A (lossy) dielectric–(lossy) dielectric interface may involve from two to four media when calculating a specific electric field component in the FDTD method. The integral form of Ampere's law can be employed to determine the proper update equation for the tangential components of the electric field on an interface. The resulting expression for the tangential electric field components is the same as in Eq.(3) with the permittivity and conductivity replaced by the arithmetic mean of the permittivities and conductivities of media at the interface [7].

For many electromagnetic-compatibility problems, frequency domain information is desired. In the present code, a sinusoidal source is applied at $t = 0$, generating transient fields. Ramping the temporal variation of the source can reduce the time necessary to achieve steady-state, but a strategy is necessary to ensure that scattered transient fields have adequately died away. APOGEE verifies that steady-state has been achieved by taking the Discrete Fourier Transform (DFT) of the electric field at selected points over the apertures. When the energy contained in the spectral component at the source frequency is 99% of the total energy, it is assumed that steady-state operation has been achieved.

Results of APOGEE for simple geometries were compared to that of the Temporal Scattering and Response (TSAR) code developed by Lawrence Livermore National Laboratory. One example was the case of an electric current density source placed symmetrically in front of a square perfectly conducting sheet. The dimensions of the sheet were $1\lambda \times 1\lambda$, and the source was located $1\lambda$ away from the sheet. The surrounding medium was free-space. The results, shown in Fig. 2, were taken along a line through the source normal to the conducting sheet. The agreement is good for both the larger fields on the source side of the conducting sheet, as well as the scattered fields in the shadow region.

The handling of dielectric interfaces and lossy dielectrics was verified by modeling an inhomogeneously filled waveguide section. The waveguide was excited in the $TE_{10}$ mode by applying "hard" sources, i.e. specifying $E_y$ over all cells of the waveguide cross-section at one point along the waveguide axis. The excitation frequency was 1.414 $f_c$, where $f_c$ was the cutoff frequency. A dielectric slab filling, one guide wavelength long, with a dielectric constant chosen such that the dielectric guide wavelength was approximately half that of the the free-space guide wavelength, was located one guide wavelength in front of the source plane. The waveguide walls were modeled as conductors, and the ends were terminated with Mur's first order boundary conditions (with the appropriate phase velocity). The waveguide cross-section was 20 x 16 cells, and the waveguide was 120 cells long (discretized at forty cells/ guide wavelength). Power computations confirmed that the one wavelength long dielectric slab was effectively behaving like a dielectric window. The electric field along the waveguide axis is shown in Fig. 3. The wavelength in the dielectric is one-half that in the filled region, and the amplitude of the wave on either side of the dielectric slab is the same. The power computations were found to

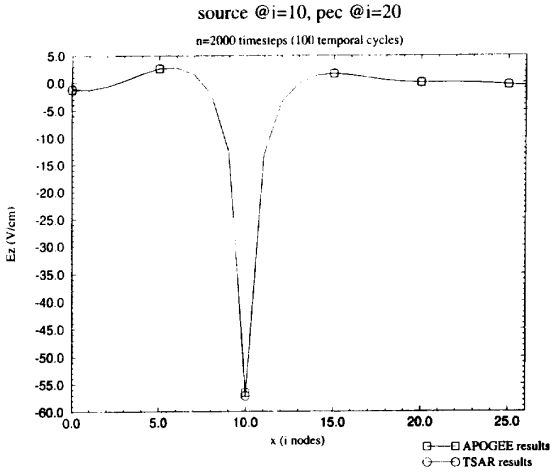


Figure 2: Comparison between the TSAR code and APOGEE.

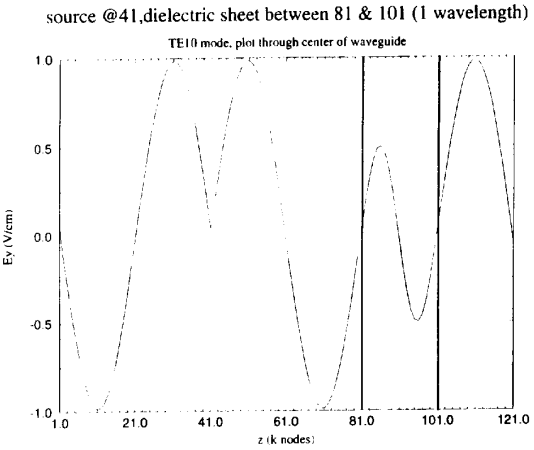


Figure 3: Waveguide results for $E_y$ using APOGEE.

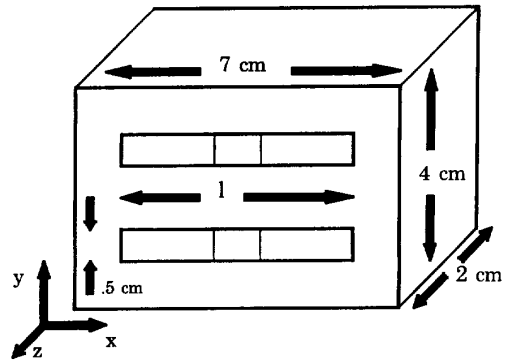


Figure 4: Mechanical enclosure with narrow apertures.

be within four percent of the theoretical calculation for a cell size of $\lambda_g/20$ (where $\lambda_g$ was the free-space guide wavelength), and within two percent for a cell size of $\lambda_g/40$.

Currently APOGEE can model perfect electric conductors, (lossy) dielectric media, electric and magnetic current density sources (soft sources), voltage sources (hard sources), sources located above conductors, and (lossy) dielectric coatings on conductors. Power and power density through apertures can be computed as well as field values for two and three dimensional representations.

# 3 Electromagnetic Compatibility Applications

The FDTD method has been employed for investigating radiation from enclosures with apertures and attached cables. A $z$-polarized electric current density source (3 $GHz$, 40 timesteps/temporal cycle) was placed symmetrically in the center of a $0.7\lambda \times 0.4\lambda \times 0.3\lambda$ enclosure with two apertures spaced a quarter wavelength apart as seen in Fig. 4. Two narrow apertures of identical length $l$ were modeled for $l$ of a half-wavelength, a quarter-wavelength, and then the two half-wavelength apertures were shorted across the middle to create four apertures two centimeters in length ($0.2\lambda$). The "short" is represented by the vertical lines across the apertures in Fig. 4. Results for $E_z$ for one timestep are shown in Fig. 5. The results are plotted along the $x$ and $y$ axes in a $z = constant$ plane one-quarter wavelength in front of the aperture. In both cases the results are plotted along a line of symmetry. Although the apertures were only a half centimeter wide (.05 $\lambda$), when the length was of resonant dimensions (half-wavelength), significantly greater fields resulted as expected. Because the apertures were narrow, the $E_x$ component of the electric field across the slot is very small, and $E_y$ is the dominant electric field component over the apertures. Using equivalence theory, the slots can be replaced with magnetic current sources with $x$-polarization. When the slot length was a half-wavelength the equivalent source is resonant resulting in efficient radiation. When the half-wavelength slots were "shorted", the surface area of the apertures was

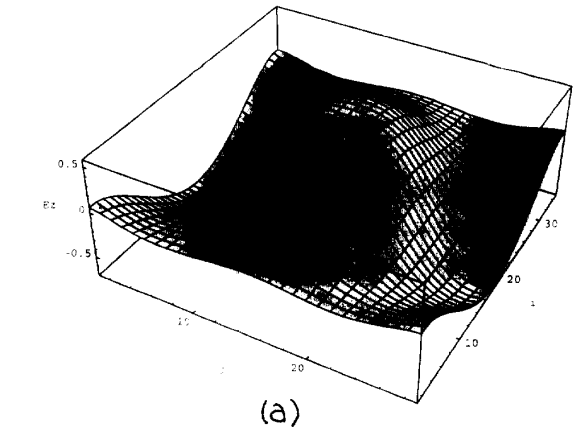

(a)

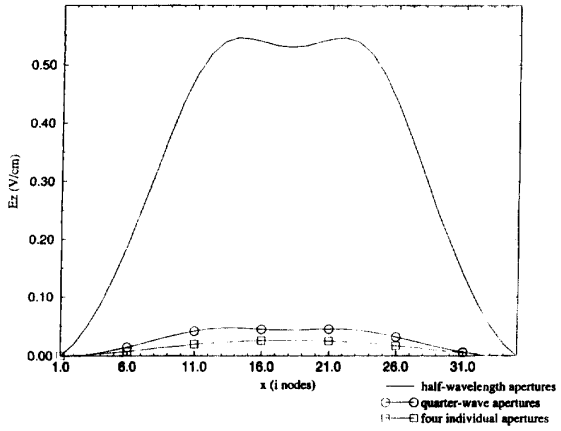


(b)

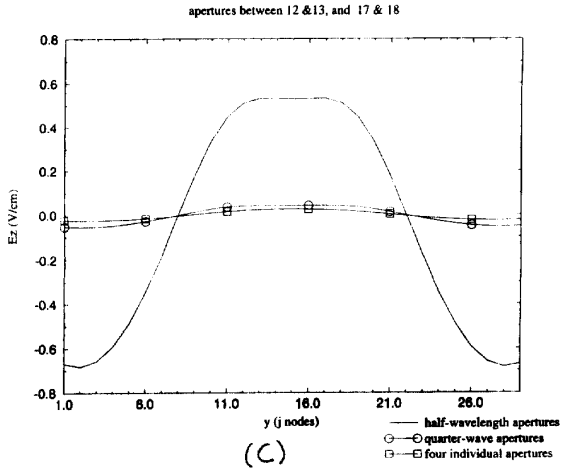


(C)

Figure 5: $E_z$ (a) through a plane one quarter-wavelength from the surface; (b) through a point in the center of the plane in the $x$ direction; and, (c) through a point in the center of the plane in the y direction for the enclosure of Figure 4.

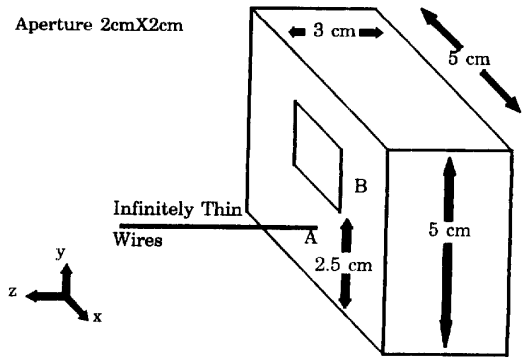


Figure 6: Mechanical enclosure with an attached shielded cable.

altered only by a small amount, but the radiation was greatly reduced due to the non-resonant length of the individual apertures. Because of the symmetry of the enclosure and location of the source within the enclosure, the slots are excited in phase and the interference is constructive in the plane of symmetry, resulting in a field maximum.

A non-resonant cavity of dimensions of $0.5\lambda \times 0.5\lambda \times 0.3\lambda$ with an aperture and attached cable is shown in Fig. 6. A square aperture $0.2\lambda$ on a side was modeled so that the aperture would be smaller than resonant dimensions. The enclosure was excited with a $z$-polarized soft electric current source located 1.5 $cm$ from the bottom of the enclosure, and centered with respect to width and depth. The source operated at 3 $GHz$ with a discretization of 40 time steps/temporal cycle. Cubic cells of 0.5 $cm$ side length were employed. The attached cable was modeled as an infinitely thin wire by setting $E_z$=0 in the unit cells through which the wire passed. The length of the cable was varied from zero to one wavelength. Two locations of the cable relative to the aperture were investigated. In one case, designated Point A in Fig. 6, the cable was positioned 1 $cm$ below the aperture. In the second case, indicated by Point B, the cable was positioned 0.5 $cm$ to the side of the aperture. The relative radiated power plotted versus wire length for both locations is shown in Fig. 7. For the attached cable positioned at Point A, the radiated power was a function of the cable length, and exhibited quarter-wavelength resonances, which indicates appreciable coupling between the aperture and cable. The enclosure with the extended cable is effectively a wire over a ground plane. Because of the finite extent of the ground plane a resonant length slightly less than a quarter wavelength is expected. When the cable at Point A was of resonant length (approximately $0.2\lambda$), the radiated power increased by approximately 5 $dB$. When the wire was located at Point B, the radiated power was virtually independent of wire length, indicating little coupling of energy from the aperture to the cable in this position.

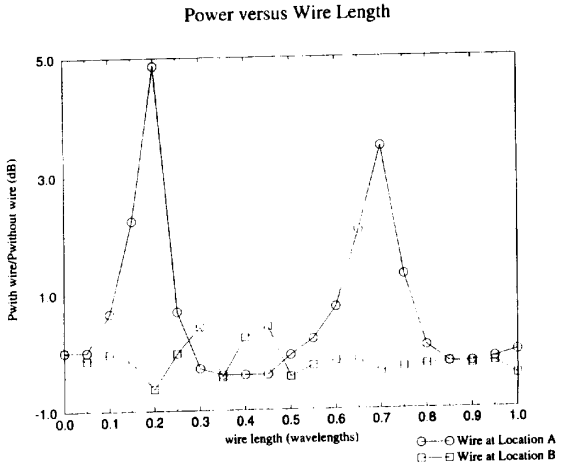


Figure 7: Radiated power versus wire length for aperture coupling to a shielded cable.

Insight into the difference in coupling from the aperture to the attached cable at positions A and B can be gained by investigating the tangential electric fields over the aperture. The tangential electric fields across the aperture are shown in Fig. 8. The aperture fields can be replaced with equivalent magnetic current sources $\overline{\mathbf{M}} = \overline{\mathbf{E}} \times \hat{\mathbf{n}}$. The magnetic current distribution across the aperture is sketched in Fig. 9. For the wire located at Point A, there is no appreciable coupling between $M_y$ and the attached cable. While a cable located at Point B is in the proper location to couple to the $y$ component of the magnetic current, the anti-symmetry of the distribution over the aperture results in a $z$ component of the electric field at the cable that is very small. The $M_x$ component of the magnetic current cannot effectively couple to a cable located Point B. For a cable located at Point A, the stronger equivalent magnetic current component $M_x$ on the side of the aperture near the cable produces a $z$ component of the electric field at the cable that is not effectively cancelled by currents on the far side of the aperture. The result is better coupling from the aperture in this case than between the $M_y$ component of the equivalent magnetic current and the cable at Point B.

# 4 Summary

A three-dimensional finite-difference, time-domain code has been developed for investigating EMI problems. The code has been developed on a rectangular mesh and can model conductors, dielectrics including loss, as well as several types of sources. The Poynting vector can be computed over a surface to yield for example, power flow across apertures in an enclosure. Radiation from enclosures has been investigated for the case of dual slots radiating in phase, and coupling from a non-resonant aperture

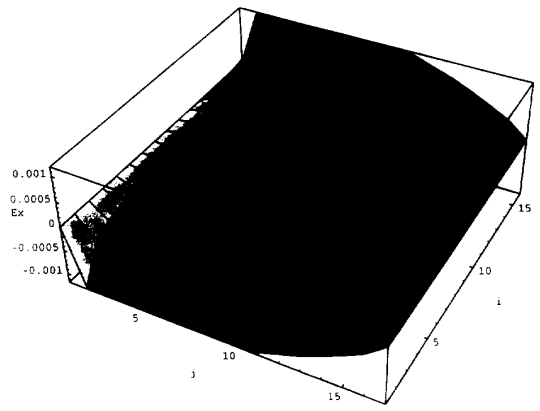


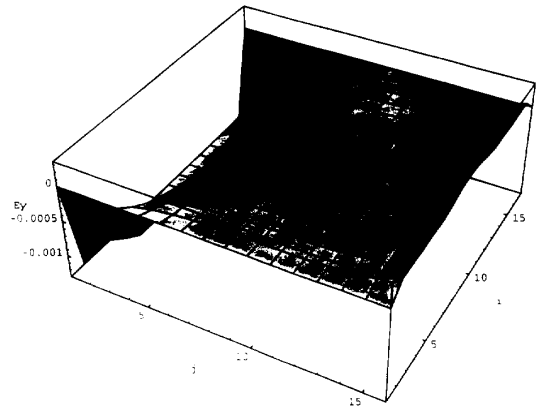


Figure 8: (a) $E_x$ across the aperture, and, (b) $E_y$ across the aperture.

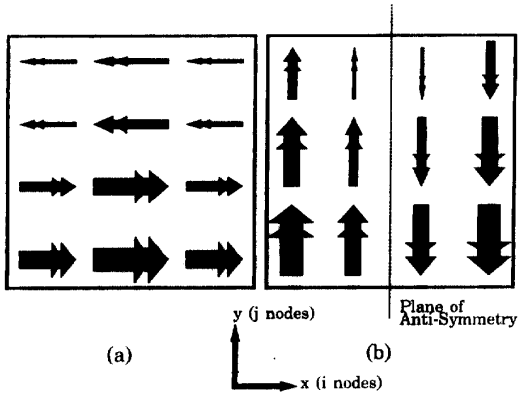


Figure 9: (a) $M_x$, and, (b) $M_y$ across the aperture.

to a shielded cable. Expected results for peak radiation from half-wavelength slots were obtained for the case of dual slots in an enclosure wall. Results of aperture coupling to a shielded cable indicated that radiation can be enhanced as a result of the wire. However, whether radiation is enhanced or not depends on the aperture distribution of the fields. It was shown that for some aperture field distributions, an external cable has relatively little effect on the radiation from the aperture. Work is currently underway to incorporate lossy-ferrites, wires with finite thickness, non-orthogonal meshes, and lumped loads into APOGEE, as well as other post-processing options.

## 5 Acknowledgements

The authors gratefully acknowledge the support of Apple Computer in pursuing this research, and the assistance of Tom Rogge with the TSAR code simulations.

## References

[1] K. S. Kunz, and R. J. Luebbers, *The Finite Difference Time Domain Method for Electromagnetics*. Boca Raton, FL: CRC Press, 1993.

[2] A. Taflove and K. R. Umashankar, "Review of FD-TD numerical modeling of electromagnetic wave scattering and radar cross section," *Proc. IEEE*, vol. 77, pp. 682-699, May 1989.

[3] K. S. Kunz, D. J. Steich, and R. J. Luebbers, "Low frequency shielding effects of a conducting shell with an aperture: response of an internal wire," *IEEE Trans. Electromagn. Compat.*, vol. 34, pp. 370-373, August 1992.

[4] K. Li, C. F. Lee, S. Y. Poh, R. T. Shin, and J. A. Kong, "Application of the FDTD method to analysis of electromagnetic radiation from VLSI heatsink configurations," *IEEE Trans. Electromagn. Compat.*, vol. 35, pp. 204-214, May 1993.

[5] B. Archambeault, and C. Brench, "Shielded air vent design guidelines for EMI modeling," *IEEE EMC Symposium Digest*, August 1993, pp. 195-199.

[6] K. S. Yee, "Numerical Solution of Initial Boundary Value Problems Involving Maxwell's Equations in Isotropic Media," *IEEE Trans. Antennas Prop.*, vol. AP-14, pp. 302-307, May 1966.

[7] K. Li, M. A. Tassoudji, R. T. Shin, J. A. Kong, "Simulation of Electromagnetic Radiation and Scattering Using a Finite Difference-Time Domain Technique," *Computer Applications in Engineering Education*, vol. 1, pp. 377-382, November 1981.

[8] G. Mur, "Absorbing Boundary Conditions for the Finite-Difference Approximation of the Time-Domain Electromagnetic-Field Equations," *IEEE Trans. Electromagn. Compat.*, vol. 23, pp. 377-382, November 1981.